Polymer Journal, Vol. 35, No. 10, pp 766—777 (2003)

Structure and Mechanical Behavior of the Mesomorphic Form in a Propylene-*b*-Poly(ethylene-*co*-propylene) Copolymer and Its Comparison with Other Thermal Treatments

Javier ARRANZ-ANDRÉS, Rosario BENAVENTE, Ernesto PÉREZ, and María Luisa CERRADA†

Instituto de Ciencia y Tecnología de Polímeros (CSIC); Juan de la Cierva 3, 28006 Madrid, Spain

(Received April 21, 2003; Accepted August 15, 2003)

ABSTRACT: Several thermal treatments have been imposed along processing to a poly[propylene-*b*-(ethylene-*co*-propylene)] and their effect on structure, thermal characterization and mechanical response has been explored. Quenching in a dry ice/methanol bath after melting has allowed to obtain a mesomorphic form due to the existence of long isotactic polypropylene (iPP) chains within the block copolymer here studied. An exhaustive analysis of such a mesophase has been performed comparing its morphological details and mechanical properties with the rest of thermal treatments. A microspherulitic superstructure is found in this mesomorphic form which leads to the lowest values in mechanical parameters, such as storage and Young moduli as well as microhardness, compared to those exhibited by the other specimens with distinct thermal histories. However, the ductility of the mesomorphic structure is the highest one, owed to the non-existence of monoclinic crystallites. A phase transition is observed at around 90°C on heating, which suggests the transformation of this mesomorphic form to the monoclinic crystalline structure.

KEY WORDS Poly(ethylene-*co*-propylene) / Mesomorphic Form / Monoclinic Crystallites /

The crystallization behavior of isotactic polypropylene (iPP) is very complicated. The morphology and properties after crystallization depend upon thermal history and the detailed microstrucutre of the polymer molecules. The iPP chains adopt a 3_1 helical conformation when crystallized from the molten state. These helical chains can organize into several different spatial arrangements giving rise to three distinct polymorphs: α-monoclinic, β-hexagonal, and γ-orthorhombic forms, depending on the crystallization conditions and catalyst used.[1—13] Cooling from the melt at low or moderate cooling rates leads usually to the formation of the thermodynamically stable α-monoclinic crystalline lattice, being this α-form the most common one.

Moreover, there is also a "mesomorphic" phase, which can be obtained by rapid quenching of molten iPP. The appearance of two broad peaks in the X-ray diffraction pattern is a characteristic of this quenched form.[14] The presence of broad, diffuse peaks in X-ray diffraction tends to suggest that the quenched structure is in a disorder state. These two peaks, however, exhibit an intermediate width between the crystal diffractions and the pattern found for a completely amorphous polypropylene.[15] Natta and Corradini[1] first pointed out that this form had an intermediate degree of ordering between the amorphous phase and the crystalline phase. They categorized it as smectic to indicate the presence of two-dimensional ordering, being better in longitudinal than in transverse chain direction.[16] However, the full evidence for the smectic phase in iPP has not been documented. The description of the mesophase can be quite confusing in the literature. In addition to the smectic phase,[1,17] other investigators described the mesomorphic phase as paracrystalline,[18,19] microcrystallites,[20—23] and nano-crystallites.[24] The term conformationally disordered crystal (condis crystal)[25] has been suggested to be more appropriate for the iPP mesomorphic form, based on its frozen liquid-like structure.

The physical properties exhibited by a given iPP are, consequently, dependent on the thermal history imposed, as aforementioned. Its numerous industrial applications require a severe control of its mechanical behavior. Stiffness and toughness are two of the most important parameters with a great practical importance, but both mechanical parameters are generally inversely proportional to each other in pure polymer, being primarily affected by the glass transition temperature (T_g). The T_g of iPP is about 0°C depending on variables such as crystallinity, crystal morphology, molecular weight, and level of isotacticity. Accordingly, an insufficient low-temperature impact strength is exhibited at low temperature by this homopolymer. To enhance the iPP impact properties, its combination with various types of elastomers has gained much attention in recent years because of its commented great industrial and commercial importance. Accordingly, blends of iPP with poly(ethylene-*co*-propylene) (EPR), ethylene–propylene–diene terpolymer rubber (EPDM), poly(styrene-*co*-butadiene-*co*-styrene) (SBS)

†To whom correspondence should be addressed (Tel: +34-91-5622900, Fax: +34-91-5644853, E-mail: mlcerrada@ictp.csic.es).

Table I. Sample characteristics of the commercial materials analyzed[a]

Sample	Isotacticity (%mmmm)	M_n	M_w	M_w/M_n	ethylene content (mol%)	MFI[b] (g/10 min)
CPE	—	77600	371300	4.8	13	7.0
iPP	91.8	87200	349000	4.0	0	8.5

[a]Data supplied by the manufacturers. [b]230 °C and 2.16 kg.

and poly(ethylene-*co*-vinyl acetate) (EVA) have been extensively analyzed[26–35] and several mechanisms of impact toughening have been proposed. In addition, the copolymerization of iPP with EPR, instead of their mixing, has been also explored and considered as an effective way to attain high-impact iPP.[36, 37]

Thermal treatment is primarily responsible for the development of a particular structure in an iPP homopolymer and, by extrapolation, for the properties exhibited. However, it is not very common in the literature to find a detailed study of the crystalline structure and properties together, being considerably more scarce the papers related, even exclusively, to the properties presented by the mesomorphic iPP. Therefore, the aim of the current work is to analyze comprehensively the effect of thermal history on the structure (WAXS, SAXS, optical microscopy, and SALS), thermal properties (DSC), viscoelastic behavior (DMTA) and mechanical response (uniaxial stretching and microhardness measurements) in a commercial polypropylene-*b*-EPR copolymer, labelled as CPE. Due to the existence of long blocks of iPP within the copolymer, the ability of developing a mesomorphic form is explored examining its properties. A comparison is established with the other different structures, obtained by changing the crystallization conditions, and their respective properties.

EXPERIMENTAL

A commercially available Ziegler–Natta catalyzed propylene-*b*-(ethylene-*co*-propylene) copolymer, supplied by Repsol YPF (Spain), has been analyzed in the current paper. The CPE copolymer has been obtained as follows: in a first reactor an isotactic polypropylene homopolymer is formed. Then, the polymerization continues in a second reactor where propylene and ethylene are fed. Therefore, a multiphasic copolymer is obtained, composed of blocks of iPP and an amorphous random ethylene-propylene copolymer (EPR), its composition being 14.1 wt% in EPR. On the other hand, the EPR component has a particular weight ratio of 65/35 ethylene/propylene. Consequently, the overall amount of ethylene is 13 mol% (9.1 wt%) both with respect to the whole CPE sample, as reported in Table I together with other characteristics of this copolymer.

A commercial iPP homopolymer has been also used for comparative purposes (see characteristics in Table I).

Films were obtained by compression molding in a Collin press between hot plates (210°C) at a pressure of 2 MPa for 4 min. Different thermal treatments were applied along crystallization. The first thermal history consisted of a cooling by immersion of the molten film inside the hot plates within a liquid nitrogen bath, labeled as QN. In the second treatment, Q, a fast cooling between plates refrigerated with water was provided to the film after its melting in the press. Finally, the S films were slowly cooled from the melt at the inherent rate of the press after switching off the power. Moreover, Q and S films were molded between two distinct types of plates: steel and teflon. Therefore, two slightly different thermal histories were attained for a given treatment, labeled as Qs, Qt, Ss, and St respectively, due to the quite different thermal conductivity exhibited by the plate materials. Moreover, another sample was prepared by melting a film of CPE in a Mettler hot stage (over a thin teflon plate) and quenching the whole set into a mixture of dry ice/methanol. This specimen will be named as QCO2. Consequently, six different thermal histories were attained: CPEQCO2, CPEQN, CPEQs, CPEQt, CPESs, and CPESt. On the other hand, the iPP homopolymer film was also compressed under identical temperature, pressure and time conditions and cooled between teflon plates refrigerated with water: sample iPPQt.

Wide-angle X-ray diffraction patterns were recorded in the reflection mode at room temperature by using a Philips diffractometer with a Geiger counter connected to a computer. Ni-filtered Cu-Kα radiation was used. The diffraction scans were collected over a period of 20 min in the range of 2θ values from 3 to 43 degrees, using a sampling rate of 1 Hz. The goniometer was calibrated with a silicon standard which was also used to determine the instrumental broadening under current experimental set-up. X-Ray crystallinity determinations were performed by subtraction of the corresponding amorphous component comparing to the totally amorphous profile of an elastomeric PP sample.[15]

The samples were also studied by small-angle X-ray scattering employing synchrotron radiation (with λ = 0.150 nm) in the beamline A2 at HASYLAB (Ham-

burg, Germany) at room temperature and at a distance of 235 cm from sample to detector. The calibration was performed with the different orders of the long spacing of rat-tail cornea (L = 65 nm). The set-up was found to cover a spacings range from 5 to 55 nm.

An optical microscope (Amplival model from Carl Zeiss Jena) was used for the morphology studies. The samples were placed between glass slides, melted above the melting point, quenched down at a given crystallization rate desired and, then, the structure was examined at room temperature under crossed polarizers.

Small angle light scattering (SALS) measurements have been performed in a similar equipment to that described previously[38] utilizing a Spectra Physics He–Ne laser source of 0.95 mW, which provided a polarized light beam with minimum divergence. The average size for the spherulites has been estimated by using the following equation

$$\overline{R} = \frac{U_{\max} \times \lambda}{4\pi \times \sin(\theta_{\max}/2)} \quad (1)$$

where λ = 632.8 nm is the wavelength of the laser light, $U_{\max}$ = 4.1 is the sphere shape factor for a four-lobe pattern at the maximum intensity and $\theta_{\max}$ is the maximum scattered angle. The scattering patterns were recorded in a JVC/SVHS625 VCR.

The thermal properties were carried out in a PerkinElmer DSC-7 calorimeter connected to a cooling system and calibrated with different standards. The sample weight ranged from 4 to 6 mg. The heating rate used was 20 °C min^{-1}. For crystallinity determinations, a value of 209 J g^{-1} has been taken as the enthalpy of fusion of the perfect α modification of iPP.[39]

Viscoelastic properties were measured with a Polymer Laboratories MK II dynamic mechanical thermal analyzer, working in a tensile mode. The temperature dependence of the storage modulus, E', loss modulus, E'', and loss tangent, tan δ, was measured at 1, 3, 10, and 30 Hz over a temperature range from −150 to 150 °C at a heating rate of 1.5 °C min^{-1}. The specimens used were rectangular strips 2.2 mm wide, around 0.17 mm thick and over 15 mm long. The apparent activation energy values were calculated according to an Arrhenius-type equation, employing an accuracy of ±1°C in the temperature assignment of E'' maxima. The frequency dependence with temperature in the relaxation mechanisms associated to the glass transition has been also considered to follow an Arrhenius behavior though it is due to cooperative motions.[40] This approximation can be made without a significant error, since the analyzed frequencies are low enough to be fitted to such a linear behavior just mentioned.

Stress–strain measurements were performed with an Instron Universal testing machine calibrated according to standard procedures and equipped with a load cell and an integrated digital display that provided force determinations. Dumb-bell shaped specimens with gauge dimensions 15 mm in length and 1.9 mm in width were punched out from the sheets with a standardized die. All of the specimens were drawn at a crosshead speed of 10 mm min^{-1} at room temperature. Young's modulus (E), yield stress (σ_y), elongation at break (ε_B) and toughness were determined from the nominal stress–strain measurements. At least four specimens were tested for each material and the mean values were reported. The error in the mean values was less than 6% except for the elongation at break and toughness estimations, these being considerably higher due to the greater inherent data scattering in the determination of these two magnitudes.

A Vickers indentor attached to a Leitz microhardness tester was used to carry out microindentation measurements. Experiments were undertaken at room temperature (23 °C). A contact load of 0.98 N and a contact time of 25 s were employed. Microhardness, MH, values (in MPa) were calculated according to the relationship:[41]

$$MH = 2 \sin 68^\circ \, P/d^2 \quad (2)$$

where P (in N) is the contact load and d (in mm) is the diagonal length of the projected indentation area.

RESULTS AND DISCUSSION

Structural Characterization

Figure 1 shows the diffraction patterns for CPEQCO2, CPESs, CPEQt, and an iPP of similar molecular weight used by comparative reason. The crystallization conditions imposed to iPP lead to the common monoclinic crystal lattice typical in this polymer synthesized with a conventional catalyst. Thus five main diffractions are obtained, corresponding to the (110), (040), (130), (111), and (041, 131) reflections of the α modification of iPP.[42] Blocks of iPP and EPR are coexisting in CPE. Since the former ones are long enough, the crystallization of those blocks occur. On the other hand, the EPR blocks do not contribute to the diffractions since they are an amorphous component exclusively incorporated by enhancing mechanical properties at low temperature. Moreover, the EPR blocks seem not to disturb the subsequent crystal lattice probably because of the long iPP chains in the CPE blocks. Therefore, the structure developed in CPE is quite similar to that exhibited by an iPP homopolymer, *i.e.*, the crystalline diffractions of the α modification are clearly observed, while no sign of the γ modification is obtained under

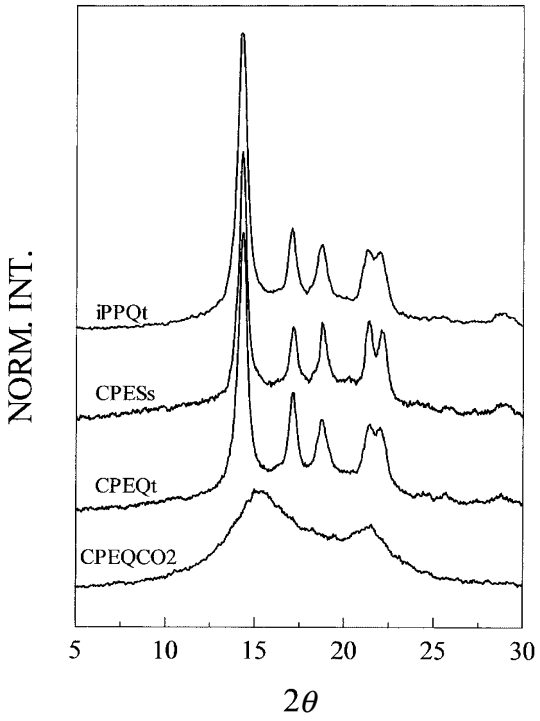

Figure 1. X-Ray diffraction patterns of CPESs, CPEQt, and CPEQCO2 at room temperature. An iPP X-ray diffractogram has been also included for comparison reason.

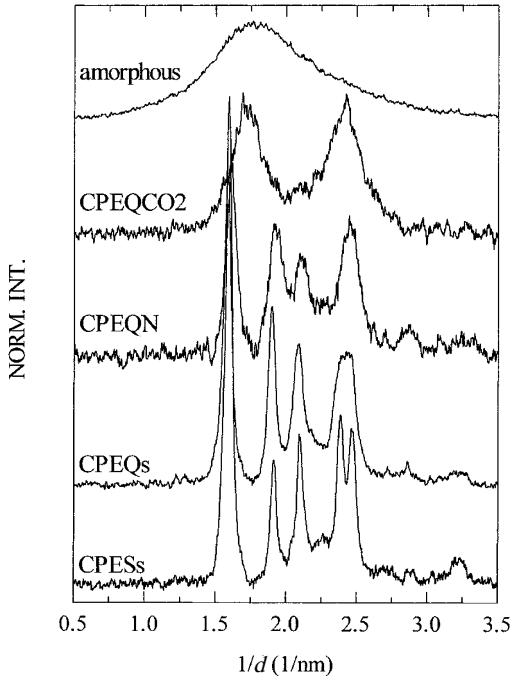

Figure 2. The amorphous halo of an atactic polypropylene,[14] the non-amorphous component for CPEQCO2 and the crystalline contributions for CPEQN, CPEQs, and CPESs.

any of the thermal treatments. The slowly cooled specimens (CPESs and CPESt) lead to more perfect crystals, so that their diffraction peaks are narrower. This can be specially noticed by the better resolution between the (111) and (041, 131) diffractions. As cooling is getting faster (CPEQa and CPEQN, and also iPP), the diffractions are broadened and the resolution between the two mentioned diffractions is worse.

In contrast, sample CPEQCO2 displays a well-differentiated diffraction pattern, which is similar to the characteristic mesomorphic form encountered in iPPs[14] and two peaks are exhibited. The appearance of these two broad and diffuse peaks tends to suggest that the structure is disordered. However, if we compare this pattern with that corresponding to a completely amorphous polypropylene,[15] shown in the upper part of Figure 2, we can see that the width of the diffractions corresponding to the mesomorphic modification is intermediate between those of the α crystals and the amorphous polymer. The absence of sharp reflections must be due to the great broadening of the diffraction lines, owed to a very small crystal size and/or a high concentration of crystalline defects, which eliminate the internal symmetry in this mesomorphic form.[43] Chains in the mesomorphic form have undergone the same conformational ordering than during the monoclinic lattice formation but the packing of helices is not as well formed as in the α crystalline phase as revealed infrared spectra.[17]

The crystallinity from the X-ray diffratograms for the different thermal histories can be assessed by subtracting the corresponding pattern of the amorphous component. We have found that the WAXS patterns corresponding to the molten CPE and reference iPP samples (acquired at 185 °C) are practically coincident (within the experimental error). Moreover, these patterns are very similar to that observed for a totally amorphous atactic polypropylene, aPP, represented in the upper curve of Figure 2, the difference being attributed to the temperature variation. For these reasons, we have estimated the crystallinity of the different samples here studied by subtracting the corresponding amount of that aPP sample. Accordingly, the pure "crystalline" profiles so obtained are presented in Figure 2. It has to be mentioned that these profiles should correspond to the pure crystalline α phase only in the case of the slowly cooled or moderately quenched samples, since when the quenching is more effective, significant proportions of mesomorphic modification are obtained. Consequently, the profile for sample CPEQCO2 corresponds to the pure mesomorphic phase (with a considerable error, owing to the uncertainty arising from the diffractions of the mesomorphic modification being rather wide), while that for sample CPEQN includes mostly α crystals but also some mesomorphic contribution, which can be estimated by comparison with the pure mesomorphic profile. The corresponding values, obtained by this procedure, for the mesomorphic and α-crystals contents are presented in Table II. From

Table II. Mesomorphic content and crystallinity estimated by WAXS and size of crystal calculated by WAXS and SAXS

Specimen	f_{meso}	$f_c^{\alpha\ form}$	$f_{total\ ordered}$	$l_c^{(110)}$(nm)	l_c (nm)
CPEQCO2	0.30	0	0.30	3.6	2.7
CEPQN	0.18	0.27	0.45	12.5	6.6
CEPQs	—	0.57	0.57	15.6	7.2
CEPQt	—	0.59	0.59	15.4	8.0
CEPSs	—	0.64	0.64	17.5	11.5
CEPSt	—	0.67	0.67	16.4	12.5
iPPQt	—	0.61	0.61	14.1	8.1

these values, it is evident that crystallinity (or the total amount of "ordered" structures: mesomorphic plus α-crystals) decreases rather appreciably as cooling rate is increased.

At this point, we have to comment on the worse quenching ability found in sample CPEQN in relation to sample CPEQCO2. As mentioned in the Experimental part, CPEQN specimen was obtained by immersing the press hot plates into liquid nitrogen. The considerable evolution of nitrogen gas and the not perfect contact between the polymer and liquid nitrogen seems to be responsible for the relatively low quenching ability exhibited by this specimen. In contrast, CPEQCO2 specimen was attained by a direct immersion of the molten polymer over a thin teflon film into dry ice/methanol. The closer contact between polymer and coolant leads to a much better quenching ability, in spite of the temperature within this latest bath being higher than in the case of liquid nitrogen one.

As commented above, the better resolved diffractions suggest a better ordering, and, consequently, longer crystallites in the slow cooled specimens. These features have been confirmed by estimation of the size of the crystallites by either WAXS or SAXS. The (110) diffraction has been utilized in the WAXS pattern for the calculation, by using the Scherrer equation,[43] of the crystal size in the (110) direction, l_c^{110}, after correction for the instrumental broadening (see experimental part). On the other hand, the crystallite size in the direction normal to the lamellae, l_c, has been estimated from the Lorentz-corrected long spacing, L, and the total crystallinity of the sample by assuming a simple two-phase model. The results for l_c^{110} and l_c are displayed in Table II. It can be observed that crystallites are smaller as crystallization rate is enlarged since a fast cooling limits development of the crystalline entities.

To get a deeper insight about the morphological details of the different crystalline structures developed, optical microscopy has been used. Figure 3 shows the optical micrographs for the different thermal treatments analyzed. The upper left picture, related to a slowly cooled specimen exhibits a typical crosshatched morphology of well-grown lamellae with spherical symmetry and highly birefringent. As cooling rate increases, as seen in the upper right picture for a quenched specimen at 40 °C min^{-1}, the change in the morphology of crystalline entities is quite substantial becoming less defined and significantly smaller confirming the results obtained from WAXS and SAXS. Faster crystallization (lower left picture) leads to observe only a mass of crystalline clots with a further reduction of their size due to

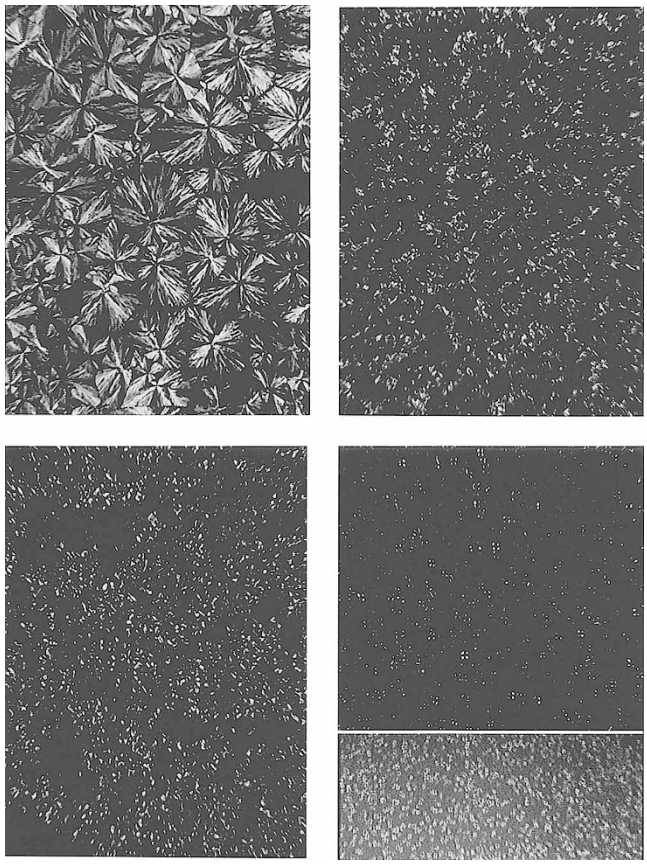

Figure 3. Morphological details at room temperature by optical microscopy under crossed polarizers in CPE: slowly cooled (upper left photo and a total width of the photograph frame of 1125 μm); quenched at 40 °C min^{-1} (upper right photo and a total width of the photograph frame of 563 μm); quenched at around 100 °C min^{-1} (lower left photo and a total width of the photograph frame of 563 μm) and mesomorphic specimen (lower right photo and a total width of the photograph frame of 563 μm. Total width of bottom inset frame of 1125 μm).

the even lower organization time of the polymer chain to develop greater and more perfect structures. Concerning the morphology observed in the mesomorphic form, no consensus has been reached as commented in the Introduction. The CPEQCO2 under study exhibits a superstructure of a very small size being composed of spherulites, as depicted in the lower right picture of Figure 3. A black background is observed since exclusively the superficial layer is shown in that photo because of the microscope objective used. To increase the resolution of that picture other photo has been taken with a smaller objective, as displayed in the bottom inset. This shows that the whole volume of CPEQCO2 is completely full of these small spherulites. To confirm the existence of this infinitesimal spherulitic morphology, a SALS analysis was performed. Such an analysis provides information about large fluctuations in density and orientation and, accordingly, about the size and the perfection of the structures.[44] A dispersion diagram Hv with a four-leaf clover symmetry was attained. The average size estimated for the spherulites by polarized light microscopy was 4–9 μm of radius while it was 3–4 μm by SALS measurements. In addition, the crystallite-like size estimated from SAXS measurements is 2.7 nm being this result in agreement with those previously found that postulated the existence of nano-crystallites.[24]

Thermal Characterization

Figure 4 shows DSC melting curves of the different samples. Different thermal transitions are observed depending upon the history provided along the preparation of the specimens. In CPESs, CPESt, CPEQs, and CPEQt three endotherms are seen along the first melting: a small step around 40 °C, followed by a small endothermic peak at about 120 °C and a sharp endotherm centered at approximately 164 °C. The former transition is associated with the melting of the crystallites annealed during the stay, after film preparation, of the material at room temperature.[45,46] This annealing peak usually appears at 15–20 °C above the annealing temperature and disappears in the second heating scan. Its intensity is dependent upon the thermal history, being smaller in the slowly cooled specimens (CPESs and CPESt) than in the faster ones (CPEQs and CPEQt). In the S samples there are less crystallites that can be improved due to the annealing effect at room temperature since such crystallites are larger, more perfect and compact than those obtained by quenching (Table II). The small endothermic transition occurring at intermediate temperatures (120 °C) is assigned to the melting of the EPR blocks. Such blocks provide the elastomeric component to the block CPE copolymer but they seems to

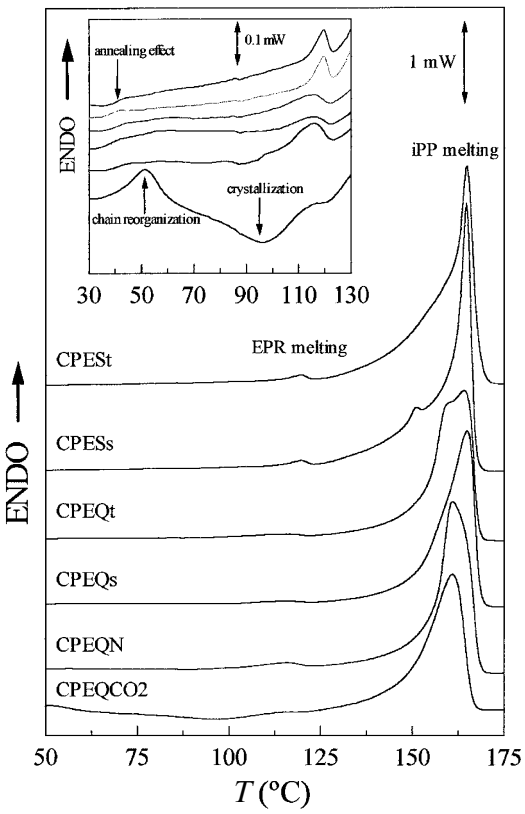

Figure 4. DSC melting curves for the different samples along first melting.

be not fully amorphous, though the enthalpy involved is quite small. Finally, the main endotherm is related to the melting of the long iPP blocks and is really formed by an overlapping of two peaks, as occurred in most iPPs. The existence of these two maxima depends on the thermal treatment imposed to the specimen during its preparation and if the crystallite formation is not rather perfect some subsequent morphological changes in the crystallite are manifested during the melting process providing a higher perfection to the crystalline structure. The behaviors of the CPE and iPP samples here studied are rather similar, and the two peaks cannot be due to two different crystalline modifications, since only the α form has been obtained in all the cases (except in the efficiently quenched samples, where the mesomorphic form is attained). Therefore, a melting-recrystallization-melting process is responsible for the occurrence of two peaks, which relative intensities are dependent either upon the heating rate or the initial crystallization conditions. The melting temperature is slightly higher in the slow cooled specimens. At lower cooling rates, the crystal thickening occurs leading to more perfect crystals due to longer times for reorganization within crystals. Moreover, the glass transition temperature, T_g, within the iPP blocks is observed at around −5 °C as listed in Table III.

On the other hand, the thermal behavior in CPE-

Table III. DSC values of the glass transition and melting temperatures, melting enthalpies and apparent calorimetric crystallinities for the iPP blocks in specimens with the different thermal treatments[a]

Sample	T_g (°C)	T_m (°C)	ΔH^{iPP} (J g^{-1})	f_c^{iPP}
CPEQCO2	−6	161	68	0.32
CPEQN	−6	161	78	0.37
CPEQs	−5	165	89	0.42
CPEQt	−6	164	90	0.43
CPESs	−5	165	105	0.50
CPESt	−5	165	103	0.49

[a]Estimated errors: temperatures ± 1°C; enthalpies ± 4 J g^{-1}; crystallinity ± 0.05.

QCO2 and CPEQN is more complex, since these specimens exhibit an additional small endotherm followed by a small exotherm. This small endothermic peak (around 40–60 °C) is assigned to the chain reorganization (or "melting") process in the mesomorphic phase whereas the exothermic event (at about 60–120°C) is ascribed to the crystallization process to develop the α-monoclinic crystallites. These two additional transitions are much more intense in CPEQCO2 than in CPEQN since the former is totally mesomorphic whereas in the latest specimen there is coexistence of a small fraction of mesomorphic form and monoclinic crystallites, as detailed in Table II.

The apparent crystallinity based on the enthalpy involved along the main melting process was also assessed for the different specimens (see Table III). However, and considering the results mentioned above, the enthalpy of the final main melting peak is not a reliable measurement of the "initial" crystallinity of the sample in those specimens most efficiently quenched, where a substantial amount of mesomorphic modification is obtained, which recrystallizes on melting into the α crystals. On the contrary, the values for the samples slowly cooled or moderately quenched are reliable. The corresponding DSC crystallinities are significantly lower than the values deduced from the X-ray diffractograms, as usual. Moreover, a clear decrease of the crystallinity is found on passing from the slowly cooled to the quenched samples, indicating the important effect of the crystallization conditions.

Viscoelastic Behavior

Figure 5 shows the viscoelastic response at 3 Hz for the different specimens with the distinct thermal treatments applied to CPE, and an iPP for comparative reasons. Due to the fact that CPE is a block copolymer, a combination of relaxation processes observed in both of the two blocks, iPP and EPR, is exhibited. Therefore, four different relaxations are shown in CPESs, CPESt, CPEQs, CPEQt, and CPEQN. Two of these mechanisms come from the EPR component (being those at the lowest temperatures and labeled γ_{EPR} and β_{EPR}) and other two processes arise from the iPP blocks within the structure of CPE, which are named as β_{iPP} and α_{iPP} in order of increasing temperatures. Moreover, an additional relaxation process, located between β_{iPP} and α_{iPP}, is exhibited by CPEQCO2. In addition to the distinct relaxations, a clear dependence of the storage modulus, E', with the thermal treatment is also observed in Figure 5. The relationship of E' and stiffness causes the variation of the former magnitude as structural variables increase the whole rigidity. Crystallinity and crystallite size are two of the most important structural variables that affect the values of E'. Consequently, CPESt and CPESs exhibit the highest E' since both the amount and the size of crystallites are the highest for these two thermal treatments. Following this thinking, it could be expected that quenched specimens, CPEQt, and CPEQs respectively, show intermediate E' values, lower than those found in the slowly cooled specimens but higher that CPEQN. However, E' for CPEQs and CPEQN presents similar values

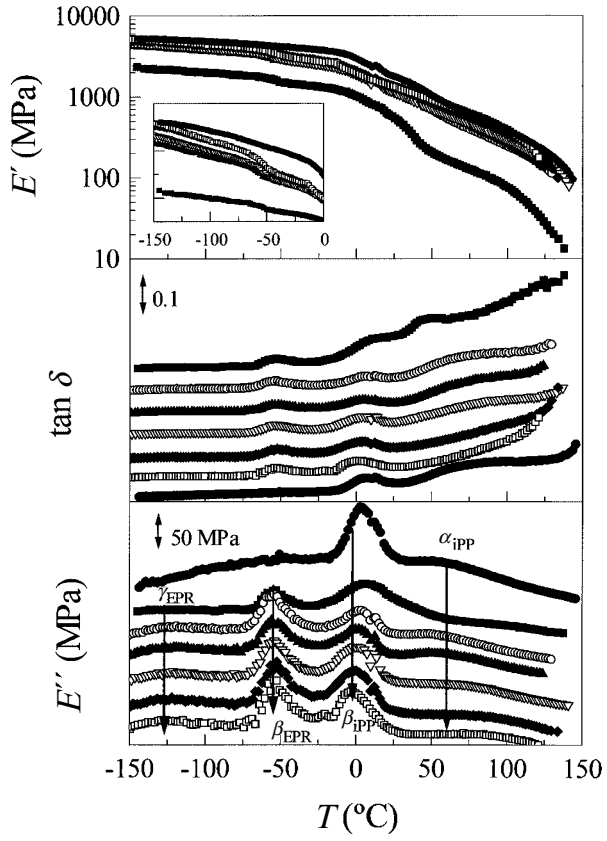

Figure 5. Temperature dependence of the either storage modulus (E') or loss modulus (E'') and of the loss tangent for the different specimens under study. From top to bottom in tan δ and E'' plots: ■; CPEQCO2, ○; CPEQs, ▲; CPEQt, ▽; CPEQN, ◆; CPESs, □; CPESt, and ●; iPP. Note that absolute values are displayed for E', while in the case of tan δ and E'' the curves have being shifted vertically for the clarity of the presentation.

Table IV. Relaxation temperatures, in E'' basis at 3 Hz, and activation energies for the different relaxation processes in the different specimens under study

Specimen	T(°C)				ΔH (kJ mol^{-1})			
	$T_{\gamma\,\mathrm{EPR}}$	$T_{\beta\,\mathrm{EPR}}$	$T_{\beta\,\mathrm{iPP}}$	$T_{\alpha\,\mathrm{iPP}}$	$\Delta H_{\gamma\,\mathrm{EPR}}$	$\Delta H_{\beta\,\mathrm{EPR}}$	$\Delta H_{\beta\,\mathrm{iPP}}$	$\Delta H_{\alpha\,\mathrm{iPP}}$
CPEQCO2	−117	−54	7	83	90	200	>400	300
CPEQs	−118	−56	2	50	85	220	>400	140
CPEQt	−120	−54	1	54	70	260	>400	130
CPEQN	−118	−54	0	58	85	220	>400	130
CPESs	−121	−53	−1	67	70	240	>400	130
CPESt	−125	−54	−3	77	55	210	>400	160
iPPQt	—	—	5	62	—	—	>400	110

and slightly higher than in CPEQt. In addition to the commented structural variables that enhance the stiffness, the residual stresses developed along film preparation are also playing a significant role. Those internal stresses become more significant as cooling rate is increased. Therefore, at initial experimental temperature, E' value is slightly higher in CPEQs than that found in CPEQt though the crystallinity and cristallite size are smaller for the former thermal history. Moreover, E' is quite similar in CPEQN than the corresponding one in CPEQs being even greater the structural differences than those displayed between CPEQt and CPEQs. CPEQCO2 shows the lower stiffness along the whole temperature range examined due to its mesomorphic character.

Regarding the different relaxation processes observed, they are analyzed separately, as follows, in order of increasing temperatures.

γ_{EPR} Relaxation. The γ_{EPR} relaxation is associated to the motion of three or more methylenic units within the EPR blocks and is related to the observed γ relaxation in polyethylene, which was firstly attributed to crankshaft movements of polymethylenic chains,[47] and currently, there is a body of opinions that support one or more of the models for restricted conformational transitions as kink formation, inversion and migration.[48–53] In the specimens under study is seen that this relaxation is shifted to lower temperatures as crystallinity and crystallite size are raised. Larger crystallites seem to impose less motion restrictions to the amorphous phase where this process takes place, as listed in Table IV. In CPEQCO2, the mesomorphic phase consisting of small spherulitic entities can be considered as being formed by many physical crosslinks and, therefore, hinders the mobility of the mentioned methylenic units. Such a hindrance is also pointed out by the diminishment of the intensity and the broadening of the relaxation time distribution of this relaxation in CPEQCO2 in comparison with the rest of thermal treatments.

β_{EPR} Relaxation. The β_{EPR} relaxation is associated with cooperative motions within the EPR amorphous component[54] in the CPE. This mechanism is not very dependent on the thermal history imposed on the CPE block copolymer either in its location or intensity (Table IV and Figure 5). The cooperative motion of long segments within the elastomeric EPR component seems to be, however, more prevented in CPEQCO2 than in the rest of specimens and, accordingly, the intensity of this β_{EPR} process is the lowest and its relaxation time distribution is the broadest. The apparent activation energy estimated agrees in values with that found in similar flexible polymers.[55,56]

The appearance of the two β_{EPR} and β_{iPP} relaxations associated both with cooperative motions, the former one within the EPR blocks, as just mentioned, and the latest process within the iPP component indicates phase separation within this CPE block copolymer, independently of the thermal treatment.

β_{iPP} Relaxation. The β_{iPP} process has been identified with the mechanism associated to the glass transition temperature of the amorphous regions within iPP blocks similarly to the relaxation appearing at the same temperature range in iPP homopolymers.[39] Similarly to the γ_{EPR} relaxation, the effect of thermal treatment on this process is significant and its maximum is moved to higher temperatures as crystallinity and crystallite size are diminished. Larger crystallites seem to impose less motion restrictions to the cooperative motion along iPP amorphous phase, as reported in Table IV. Consequently, CPEQCO2 exhibits its maximum shifted at the highest temperature. Moreover, the relaxation time distribution involved in this mechanism for CPEQCO2 is considerably much broader than for specimens with the other thermal histories. On the one hand, the higher hindrance imposed by its intrinsic morphology and, on the other hand, the overlapping of this process with an additional relaxation, which exclusively takes place in CPEQCO2 at around 45 °C on tan δ plot (see Figure 5), are responsible for such a broadening. The motion of those spherulitic entities allocated all along the mesomorphic phase probably causes this extra relaxation.

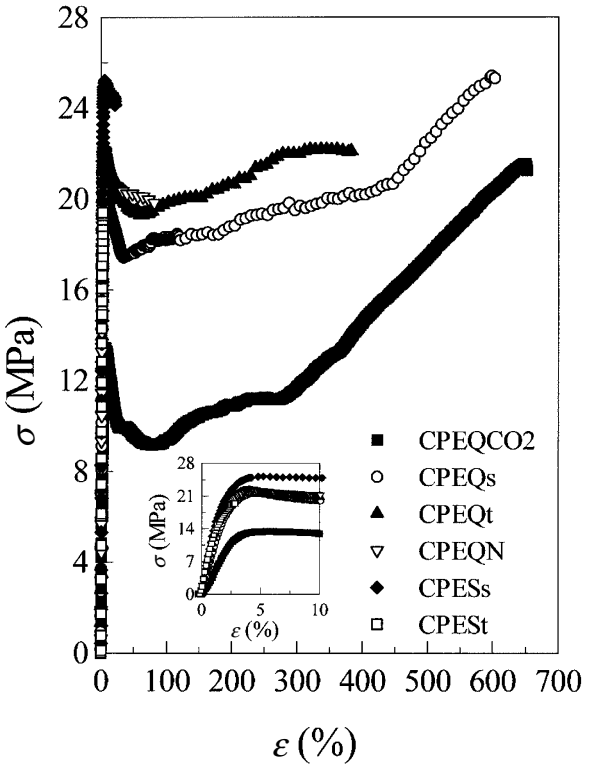

Figure 6. Stress–strain curves for the different samples stretched at room temperature and 10 mm min^{-1}.

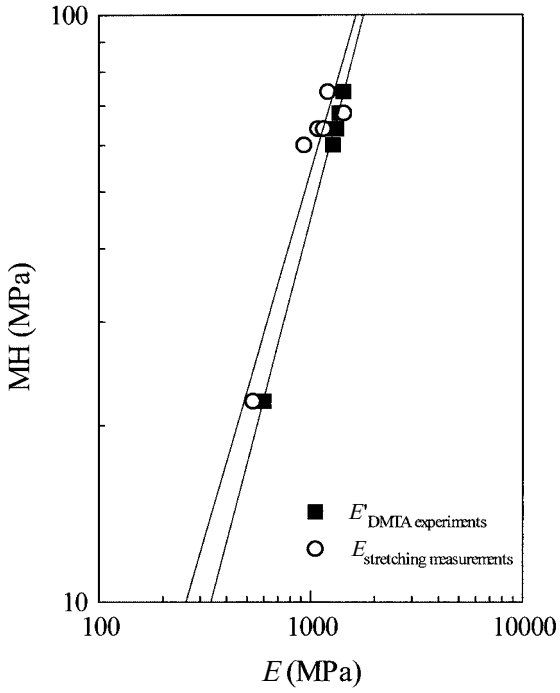

Figure 7. Relationship between *MH* and Young's modulus.

α_{iPP} Relaxation. The α_{iPP} relaxation exhibited by specimens with the different thermal treatment is assigned to movements within the monoclinic crystallites, analogously to the relaxation occurring in an iPP homopolymer at the same temperature range. The effect of the thermal history on its location has been reported for iPP.[39] A shift to higher temperatures is observed as crystallinity and crystal size increase. This tendency is altered for CPEQCO2. Initially, there are not monoclinic crystallites in this specimen. However, they are obtained from the mesomorphic form after the phase transformation in the 65 to 85°C temperature range. Consequently, the motion of the monoclinic crystallites can take place after their formation and the α_{iPP} relaxation start to occur at around 75°C, *i.e.*, it is significantly shifted to higher temperatures. In the case of CPEQN, there are a fraction of mesomorphic entities but the ordered structure is mainly due to monoclinic crystals and, therefore, this relaxation process starts at temperatures close to those observed in CPEQs and CPEQt.

Mechanical Response

Stress–Strain Behavior. Figure 6 shows the stress–strain curves of different CPE specimens stretched at room temperature and at strain rate of 10 mm min^{-1}. Young modulus (E), yield stress (σ_Y), and toughness are determined from those curves and their values reported in Table V. All these mechanical parameters investigated are dependent on thermal treatment. The higher crystallinity and the more compact and largest crystallites developed in the slowly cooled specimens introduce a higher rigidity. Therefore, on the one hand, the modulus and yield stress for specimens with this thermal history are the highest ones and, on the other hand, the elongation at break significantly diminishes comparing with the other treatments (see Figure 6). Regarding CPEQN specimen, it can be observed in Table V and Figure 7 that its mechanical parameters show values unexpected taking into account exclusively its morphological characteristics. For instance, a higher value is obtained for the Young modulus and a lower one for the deformation at break in relation to CPEQs and CPEQt samples. Our tentative explanation is that the residual stresses introduced along processing provoke this unexpected behavior.

The typical cold deformation process is only exhibited in CPEQs and CPEQCO2 though the neck propagation is quite irregular in both of them. The morphological differences, monoclinic crystallites in the former specimen and mesomorphic form in the latest one, significantly affect the value of Young modulus, which is related to the stiffness, pointing out the diminishment of the rigidity within CPEQCO2. The yield stress is also considerably decreased in the mesomorphic sample. A common feature of all the specimens is their whitening as they are stretched. This opacity points out the formation of microvoids[57] during the deformation process, which is also significantly dependent on

Table V. Mechanical parameters of the different specimens analyzed at 21°C and stretched at 10 mm min^{-1}: Young's modulus, E; yield stress, σ_Y; deformation at break, ε_B; toughness, T; microhardness, MH.

Specimen	E (MPa)	σ_Y(MPa)	ε_B(%)	T (KJ m^{-2})	MH (MPa)
CPEQCO2	530	14	650	1400	22
CPEQs	930	22	500	1500	60
CPEQt	1100	21	350	1200	64
CPEQN	1150	22	120	360	64
CPESs	1450	24	16	50	68
CPESt	1200	—	3	10	74

thermal treatment imposed to CPE copolymer. Slowly cooled samples become white just when the drawing process starts. CPEQt, CPEQs, CPEQN whiten around yield stress takes place whereas the whitening is observed in CPEQCO2 along the necking propagation.

Toughness is other important mechanical property. Its concept might be defined in several ways, one of which is in terms of the area under the stress–strain curve.[58] Toughness is, therefore, an indication of the energy that a material can absorb before breaking. Moreover, a significant dependence upon thermal treatment is expected due to the distinct morphology developed. Accordingly, CPEQCO2 and CPEQs are the tougher specimens (Table V). Though CPEQCO2 is the specimen with the largest deformation at break and strain-hardening process starts at lower deformation values, its less stress level compared to CPEQs is responsible of its slightly smaller toughness.

Microhardness Measurements. MH is other significant mechanical magnitude in polymers, which measures the resistance of the material to plastic deformation and, accordingly, provides an idea about local strain. MH involves a complex combination of properties (elastic modulus, yield strength, strain hardening, toughness). Its dependency upon thermal treatment is quite analogous to that observed for Young modulus in CPE block copolymer under study, as detailed in Table V. A direct relationship is commonly found between the Young's modulus and MH[40] and the following empirical equation has been proposed:

$$MH = a\,E^b \qquad (3)$$

where a and b are constants. This equation is also fulfilled by many systems[56, 59, 60] in a very broad range of MH and E values: from thermoplastic elastomers to very rigid polymers. Figure 7 show a good linear relationship between MH and either E or E' in those specimens with monoclinic crystalline structure. CPEQCO2 does follow that linearity though is located at lower values due to its mesomorphic morphology at room temperature. On the other hand, the relationship between microhardness and total crystallinity (mesomorphic plus α crystals fraction), $f_{\text{total ordered}}$, and crystal size, l_c, have been represented in Figure 8 since they are two very significant structural parameters that affect rigidity and, consequently, microhardness. The difference in morphological details is again pointed out and, accordingly, CPEQCO2 exhibits the lowest values.

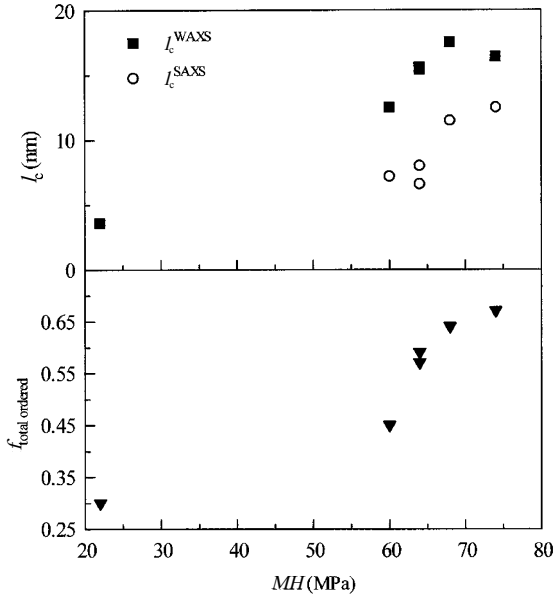

Figure 8. Relationships between X-ray crystallite size, l_c, (upper plot) and total crystallinity, $f_{\text{total ordered}}$, (lower plot) with microhardness in the different specimens.

CONCLUSIONS

A microespherulitic superstructure is found in the mesomorphic form which leads to the lowest values in mechanical parameters, such as either storage or loss moduli as well as microhardness, compared to those exhibited by the other specimens with distinct thermal histories. However, the ductility of this mesomorphic structure is the highest one, owed to the non-existence of monoclinic crystallites. A phase transition is observed at around 90 °C on heating, which suggests the transformation of this mesomorphic form to the monoclinic crystalline structure.

Acknowledgments. The financial support of CAM and CICYT (Projects 07N/0093/2002 and MAT2001-

2321) and the supply of the CPE copolymer by Repsol YPF (Spain) is gratefully acknowledged. J. Arranz-Andrés is grateful to the CICYT (project MAT2001-2321) for his financial support. The synchrotron work (in the polymer line of Hasylab at DESY, Hamburg) was supported by the IHP Programme "Access to Research Infrastructures" of the European Commission (Contract HPRI-CT-1999-00040). We thank the collaboration of the Hasylab personnel, and specially Dr. S. Funari and Dr. A. Meyer, responsibles of the polymer beamline. We also thank the EU COST programme, under Action D17. Finally, we would like to thank to Dr. C. Marco his help in the SALS experiments.

REFERENCES

1. G. Natta and P. Corradini, *Nuovo Cimento Suppl.*, **15**, 40 (1960).
2. H. D. Keith, F. J. Padden Jr., N. M. Walter, and H. W. Wyckoff, *J. Appl. Phys.*, **30**, 1485 (1959).
3. A. Turner Jones, J. M. Aizlewood, and D. R. Beckett, *Makromol. Chem.*, **75**, 134 (1964).
4. S. V. Meille, D. R. Ferro, S. Brückner, A. J. Lovinger, and F. J. Padden, *Macromolecules*, **27**, 2615 (1994).
5. E. J. Addink and J. Beintema, *Polymer*, **2**, 185 (1961).
6. S. V. Meille, S. Brückner, and W. Porzio, *Macromolecules*, **23**, 4114 (1990).
7. E. Pérez, D. Zucchi, M. L. Sacchi, F. Fornili, and A. Bello, *Polymer*, **40**, 675 (1999).
8. A. Turner-Jones, *Polymer*, **12**, 487 (1971).
9. R. Thomann, C. Wang, J. Kressler, and R. Mulhaupt, *Macromolecules*, **29**, 8425 (1996).
10. R. Campbell and P. Phillips, *Polymer*, **34**, 4809 (1993).
11. B. Lotz, J. Wittman, and A. Lovinger, *Polymer*, **37**, 4979 (1996).
12. S. Bruckner and S. Meille, *Nature*, **340**, 455 (1989).
13. K. Mezghani and P. Phillips, *Polymer*, **38**, 5725 (1997).
14. R. Androsch and B. Wunderlich, *Macromolecule*s, **34**, 5950 (2001).
15. S. Mansel, E. Pérez, R. Benavente, J. M. Pereña, A. Bello, W. Röll, R. Kirsten, S. Beck, and H.-H. Brintzinger, *Macromol. Chem. Phys.*, **200**, 1292 (1999).
16. a) D. C. Bassett and R. H. Olley, *Polymer*, **25**, 935 (1984).
    b) R. H. Olley and D. C. Bassett, *Polymer*, **30**, 399 (1989).
17. C. C. Hsu, P. H. Geil, H. Miyaji, and K. Asai, *J. Polym. Sci., Part B: Polym. Phys. Ed.*, **24**, 2379 (1986).
18. R. L. Miller, *Polymer*, **1**, 135 (1960).
19. R. Hosemann and W. Wilke, *Makromol. Chem.*, **118**, 230 (1968).
20. J. A. Gailey and R. H. Ralston, *SPE Trans*, **4**, 29 (1964).
21. G. Bodor, M. Grell, and A. Kallo, *Faserforsch Textil Tech.*, **15**, 527 (1964).
22. G. Caldas, G. R. Brown, R. S. Nohr, J. G. MacDonald, and L. E. Raboin, *Polymer*, **35**, 899 (1994).
23. N. S. Murthy, H. Minor, C. Bednarczyk, and S. Krimm, *Macromolecules*, **26**, 1712 (1993).
24. A. Ferrero, E. Ferracini, A. Mazzavillani, and V. Malta, *J. Macromol. Sci., Phys.*, **B39**, 109 (2000).
25. J. Grebowicz, J. F. Lau, and B. Wunderlich, *J. Polym. Sci., Polym. Symp.*, **71**, 19 (1984).
26. A. K. Gupta, B. K. Ratnam, and K. R. Srinivasan, *J. Appl. Polym. Sci.*, **45**, 1303 (1992).
27. Y. Kim, W. J. Cho, and C. S. Ha, *Polym. Eng. Sci.*, **35**, 1592 (1995).
28. C. L. Wang, S. J. Wang, and Z. N. Qi, *J. Polym. Sci., Part B: Polym. Phys.*, **34**, 193 (1996).
29. T. Inoue and T. Suzuki, *J. Appl. Polym. Sci.*, **59**, 1443 (1996).
30. A. Sengupta and B. B. Konar, *J. Appl. Polym. Sci.*, **70**, 2155 (1998).
31. A. Van der Wal and R. J. Gaymans, *Polymer*, **40**, 6045 (1999).
32. A. Van der Wal, A. J. J. Verheul, and R. J. Gaymans, *Polymer*, **40**, 6057 (1999).
33. A. Van der Wal and R. J. Gaymans, *Polymer*, **40**, 6067 (1999).
34. S. H. Jafari and A. K. Gupta, *J. Appl. Polym. Sci.*, **78**, 962 (2000).
35. C. Hungjun, L. Xiaolie, C. Xiangxu, M. Dezhu, W. Jianmin, and T. Hongsheng, *J. Appl. Polym. Sci.*, **71**, 103 (1999).
36. L. Wang and B. Huang, *J. Polym. Sci., Part B: Polym. Phys.*, **29**, 1447 (1991).
37. H. Mori, M. Yamahiro, K. Tashino, K. Ohnishi, K. Nitta, and M. Terano, *Macromol, Rapid Commun.*, **16**, 247 (1998).
38. a) R. S. Stein ed., "New Methods of Polymer Characterization", Wiley-Interscience, New York, N.Y., 1964.
    b) R. S. Stein and M. Srinivasarao, *J. Polym. Sci., Part B: Polym. Phys.*, **31**, 323 (1993).
39. J. R. Isasi, L. Mandelkern, M. J. Galante, and R. G. Alamo, *J. Polym. Sci., Part B: Polym. Phys.*, **37**, 323 (1999).
40. N. G. McCrum, B. E. Read, and G. Williams, "Anelastic and Dielectric Effects in Polymeric Solids", Dover Publications, Inc., New York, N.Y., 1991.
41. F. J. Baltá Calleja, *Adv. Polym. Sci.*, **66**, 117 (1985).
42. Z. Mencik, *J. Macromol. Sci., Phys.*, **B6**, 101 (1972).
43. L. E. Alexander, "X-ray Diffraction Methods in Polymer Science", ed. Wiley-Interscience, New York, N.Y., 1969.
44. N. V. Pogodina, S. K. Siddiquee, J. W. Van Egmond, and H. H. Winter, *Macromolecules*, **32**, 1167 (1999).
45. S. Bensason, J. Minick, A. Moet, S. Chum, A. Hiltner, and E. Baer, *J. Polym. Sci., Part B: Polym. Phys.*, **34**, 1301 (1996).
46. A. Alizadeh, L. Richardson, J. Xu, and H. Marand, *Macromolecules*, **32**, 6221 (1999).
47. T. F. Schatzki, *J. Polym. Sci.*, **57**, 496 (1962).
48. R. F. Boyer, *Rubber. Chem. Technol.*, **36**, 1303 (1963).
49. R. H. Boyd and R. S. Breitling, *Macromolecules*, **7**, 855 (1974).
50. R. H. Boyd, *J. Polym. Sci., Part B: Polym. Phys.*, **13**, 2345 (1975).
51. R. H. Boyd, R. H. Gee, J. Han, and Y. Jin, *J. Chem. Phys.*, **101**, 788 (1994).
52. J. Han, R. H. Gee, and R. H. Boyd, *Macromolecules*, **27**, 7781 (1994).
53. Y. Jin and R. H. Boyd, *J. Chem. Phys.*, **108**, 9912 (1998).
54. M. Yamaguchi, H. Miyata, and K. Nitta, *J. Appl. Polym. Sci.*, **62**, 87 (1996).
55. M. L. Cerrada, R. Benavente, and E. Pérez, *Macromol. Chem. Phys.*, **202**, 2686 (2001).
56. M. L. Cerrada, J. L. de la Fuente, M. Fernández-García, and

E. L. Madruga, *Polymer*, **42**, 4647 (2001).
57. Y. Liu and R.W. Truss, *J. Polym. Sci., Part B: Polym. Phys.*, **32**, 2037 (1994).
58. R. A. Duckett in "Structure and Properties of Oriented Polymers", I. M. Ward, ed, Applied Science Publishers, London, 1975, chapt. 11.
59. V. Lorenzo, J. M. Pereña, and J. M. G. Fatou, *Makromol. Chem.*, **172**, 25 (1989).
60. R. Benavente, E. Pérez, and R. Quijada, *J. Polym. Sci., Part B: Polym. Phys.*, **39**, 277 (2001).